

PEG-Grafted Graphene/PLLA Nanocomposites: Effect of PEG Chain Length on Crystallization Kinetics of PLLA

Samira Karimi, Ismaeil Ghasemi, Foroud Abbassi-Sourki,* Mazen Samara, and Nicole.R Demarquette*

Cite This: *ACS Omega* 2022, 7, 31197–31204

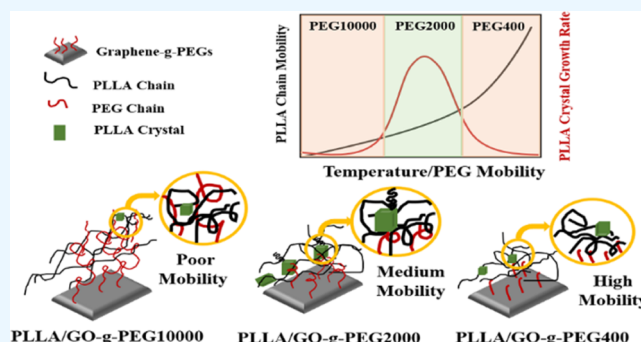
Read Online

ACCESS |

Metrics & More

Article Recommendations

ABSTRACT: Poly-L-lactic acid (PLLA) nanocomposites containing graphene oxide (GO), modified with different chain lengths of poly(ethylene glycol) (PEG) (400, 2000, and 10 000 g/mol), were prepared by solution casting. The effect of the PEG chain length and nanoparticle content (0.5, 1, and 1.5 wt %) on the nucleation, crystal growth rate, and overall crystallization rate, under isothermal conditions, was then evaluated. The results showed that, in samples containing GO modified with 400 g/mol of PEG, the nucleation density increased as a function of a modified nanoparticle concentration. In the case of the samples containing GO modified with PEG of a molar mass of either 2000 or 10 000 g/mol, the nucleation density exhibited a maximum at a concentration of 1 wt %. Furthermore, the addition of graphene oxide modified with poly(ethylene glycol) of a molar mass of 2000 g/mol resulted in the largest nucleation, fastest crystal growth, and highest overall crystallization rate, for all concentrations. The results were explained in light of the steric hindrance between the modified nanoparticles.



1. INTRODUCTION

For the last 20 years, poly-L-lactic acid (PLLA) has attracted considerable interest because of its biocompatibility and biodegradability properties,^{1,2} which make it a versatile candidate as a substitute for petroleum-based polymers.^{3–5} However, weak mechanical and gas barrier properties, poor processability, and slow crystallization rate have limited its use for several applications.⁶ Since the PLLA properties are greatly influenced by its crystallization characteristics such as crystallization kinetics and degree of crystallinity, the overall crystallization rate of PLLA needs to be improved.

The crystallization process of semicrystalline polymers consists of two steps: (1) nucleation which includes alignment of polymer segments and cluster formation and (2) crystal growth which is controlled by long-range diffusion and organization into lamellae.⁷ The current strategies to improve the overall crystallization rate of a given polymer are therefore based on enhancing nucleation and improving chain mobility.¹ The nucleation can be improved when nanoparticles are added to a polymer. Nanoparticles such as carbon nanotubes (CNTs),^{8,9} graphene,¹⁰ and nanoclays^{11–13} are commonly used as nucleating agents. They decrease the nucleation activation energy by providing heterogeneous nucleation sites. In particular, graphene, a one-atom-thick, two-dimensional material, has received particular interest in both academic and industrial research due to its excellent thermomechanical and electrical properties.^{14–16} Its huge specific surface area and

large aspect ratio are two important characteristics of an effective and remarkable nucleating agent for improving polymer crystallization. Concomitantly, the chain mobility can be improved using plasticizers such as PLA oligomers,¹⁷ PEG, citrate ester,¹⁸ and triphenyl phosphate (TPP),¹⁹ leading to a higher crystal growth rate. In particular, PEG has shown good compatibility with PLLA even at large loadings and significantly impacted the crystallization rate of PLLA.^{18–21}

Several researchers have suggested to harness the effect of nanofillers and plasticizers on crystallization to enhance both nucleation and growth rate. Their results indicated that plasticizers, in addition to aiding the chain mobility, improved nanofiller dispersion, resulting in further nucleation and crystal growth rate.^{1,22–25} However, the presence of plasticizers also leads to a reduction in mechanical properties. To counter the reduction of mechanical properties, Xu et al.²⁶ suggested the use of graphene oxide (GO), to which PEG had been covalently grafted, as an additive to enhance the crystallization behavior of PLLA. They compared their results to those

Received: May 31, 2022

Accepted: August 11, 2022

Published: August 23, 2022



obtained by adding PEG and GO, separately. They concluded that the suggested approach led to a remarkable acceleration in the crystal growth rate at a much lower concentration of GO-g-PEG, compared to incorporating PEG and GO, separately. They attributed this to the fact that PEG grafted to GO (1) improved the dispersion of GO within PLLA, enhancing the nucleation rate, and (2) enhanced the PLLA chain mobility, resulting in the acceleration of the lamellae growth rate.

More recently, Karimi et al.²⁷ investigated the kinetics of PLLA crystallization in the presence of two types of nanoparticles: GO and GO-g-PEG with various concentrations. Their kinetic analyses and morphological observations indicated that GO-g-PEG enhanced the crystallization rate as well as the nucleation rate of PLLA. The improved dispersion of GO-g-PEG in the PLLA stemming from the higher compatibility of PEG chains with PLLA ones was accounted as the main cause of this behavior. The crystallization behavior of PLLA in the presence of polymer-grafted nanoparticles is, however, still an interesting and challenging area of research as the underlying phenomena that govern the role of the polymer-grafted nanoparticles are still far from being understood.

This study was undertaken to examine the effect of the PEG chain length of GO-g-PEG on the crystallization behavior of PLLA/GO-g-PEG nanocomposites. Three different molecular weights of PEG were used to show how the chain length of GO-g-PEG affects the chain mobility of PLLA and the performance of GO-g-PEG as a nucleating agent.

2. EXPERIMENTAL SECTION

2.1. Materials. Commercial grade PLLA (4032D), with a D-isomer content of 2 wt % and a molar mass of 2.23×10^5 g/mol, was obtained from NatureWorks. PEG with a molar mass of 400, 2000, or 10 000 g/mol was purchased from Merck. Graphene nanoplatelets (GNPs) were purchased from Advanced Chemicals Supplier (ACS) Material. The GNP particles included aggregates of submicron platelets with a diameter of about 65 μm and a typical thickness of 2–10 nm, as can be seen in Figure 1. For graphene oxidation, sulfuric acid (H_2SO_4), hydrochloric acid (HCl), sodium nitrate (NaNO_3), and potassium permanganate (KMnO_4) were used. For the PEG-grafting reaction, dimethyl sulfoxide (DMSO) was used. For preparing PLLA nanocomposites, dimethyl formamide (DMF) was used. All of the above-mentioned solvents and powders were obtained from Merck.

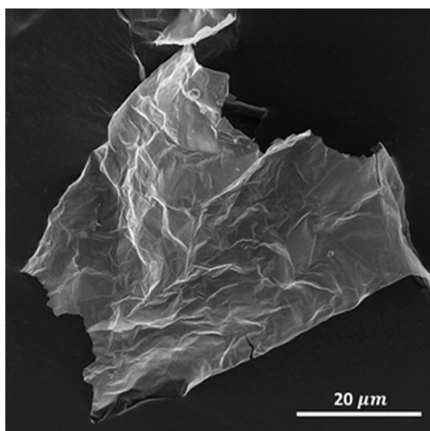


Figure 1. SEM image of graphene.

1,1'-Carbonyldiimidazole (CDI) used as an activation agent in the PEG-grafting reaction was obtained from Sigma-Aldrich.

2.2. Sample Preparation. The complete details of sample preparation including the oxidation of GNPs to obtain oxidized graphene (GO) and the grafting of PEG on GO along with purification steps can be found elsewhere.²⁷ The PLLA/GO and PLLA/PEG-g-GO nanocomposites were prepared by solution casting.²⁷

The code for the PLLA nanocomposites prepared in this paper is x - y , where x is the molecular weight of the PEG grafted on graphene oxide and y is the weight percent of nanoparticles. For example, 400-0.5 corresponds to the PLLA nanocomposites containing 0.5 wt % of GO grafted with PEG400. All sample compositions along with designations are presented in Table 1.

Table 1. Abbreviation of Different Samples and Their Compositions

sample code	GO-g-PEG400	GO-g-PEG2000	GO-g-PEG10000
400-0.5	0.5	0	0
400-1	1	0	0
400-1.5	1.5	0	0
2000-0.5	0	0.5	0
2000-1	0	1	0
2000-1.5	0	1.5	0
10 000-0.5	0	0	0.5
10 000-1	0	0	1
10 000-1.5	0	0	1.5

2.3. Characterization. The modification of GO was evaluated using FTIR-ATR, XRD, and TGA. FTIR-ATR spectra were obtained by a Perkin–Elmer FTIR spectrometer over a wave number in the range of 400–4000 cm^{-1} , with a resolution of 4 cm^{-1} and a number scan of 10. X-ray diffraction measurements were carried out by means of an XRD X'Pert³ Panalytical with Cu $K\alpha$ radiation ($\lambda = 1.542 \text{ \AA}$) operated at 45 kV and 40 mA. Data were recorded in the 2θ range of 5–40° at a scan rate of 1.2°/min. TGA has been performed using a TGA/DSC1 Mettler-Toledo (Switzerland). The experiment was carried out in an atmosphere of nitrogen at a heating rate of 10 °C/min, and the mass loss was recorded.

The dispersion of nanoparticles within the PLLA matrix was assessed by field emission scanning electron microscopy (FE-SEM). For that, the samples were cryofractured in liquid nitrogen, and the fracture surface was then coated with gold and analyzed with a MIRA 3 (7 kV), TESCAN system.

The viscoelastic properties of nanocomposites were examined to achieve a better understanding of the dispersion of nanoparticles within the PLLA matrix. For that, the samples were subjected to small-amplitude oscillatory shear using an MCR 501 rheometer from Anton Paar under N_2 atmosphere at a temperature of 190 °C, with parallel-plate geometry. The diameter and plate gap were selected as 25 and 1 mm, respectively.

The crystallization of nanocomposites was studied by microscopy and differential scanning calorimetry. The spherulite growth and its morphology were studied using a polarized optical microscope (POM) (Carl Zeiss Jena JENAPOL Instrument), equipped with a hot stage. The samples were heated up to 190 °C at a heating rate of 5 °C/min and kept at this temperature for 5 min to eliminate any thermomechanical history. They were then cooled to a

crystallization temperature of 130 °C at a cooling rate of 30 °C/min and held for 30 min for isothermal crystallization. The micrographs were used together with ImageJ software to measure the size of the spherulite as a function of time, which was then used to infer the crystal growth rate. The nucleation density was inferred from the number of spherulites within a certain area.

A Mettler-Toledo (Switzerland) differential scanning calorimeter was used to investigate the isothermal crystallization of the nanocomposites under a nitrogen atmosphere. To erase their thermal history, the samples were first annealed at 190 °C for 5 min, then quenched to a crystallization temperature of 130 °C at a rate of 30 °C/min, and finally kept at this temperature for 30 min to complete the crystallization. From the curves of heat flow as a function of time, it was possible to infer the relative crystallinity as a function of time, from which the onset of crystallization and the half-time of crystallization were determined. The half-time of crystallization is referred to as overall crystallization.

3. RESULTS

3.1. Characterization of GO-g-PEG with Different Lengths of PEG. To verify that the oxidation and grafting reactions had been performed properly, various techniques including XRD, FTIR, and TGA were used. Figure 2 presents

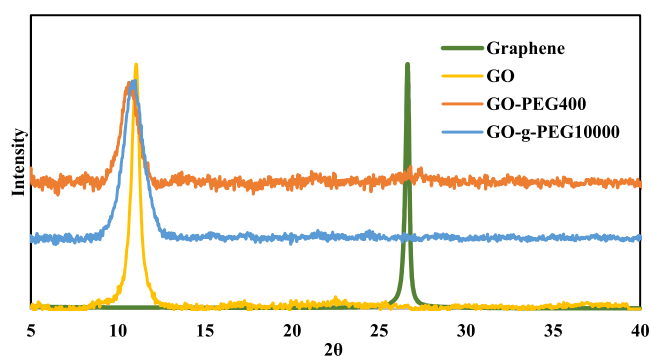


Figure 2. XRD pattern of graphene, GO, GO-g-PEG400, and GO-g-PEG10000.

the XRD pattern of graphene, GO, GO-g-PEG400, and GO-g-PEG10000. As can be observed, the characteristic peaks of graphene, GO, GO-g-PEG400, and GO-g-PEG10000 appear at $2\theta = 26.6$, $2\theta = 11.08$, $2\theta = 10.6$, and $2\theta = 11.02$, respectively.

The decrement in the characteristic peaks of GO, GO-g-PEG400, and GO-g-PEG10000 is a sign of increasing D-spacing between graphene sheets related to oxidation and the presence of oxygen-containing groups and PEG chains on the surface of different nanoparticles.^{27–30} The results of GO-g-PEG2000 have been shown in our previous work.²⁷

Chemical changes in graphene, during oxidation and grafting, were studied using ATR-FTIR. Figure 3 displays the FTIR spectra of GO, GO-g-PEG400, and GO-g-PEG10000. In the GO spectrum, the characteristic peak at 1718 cm^{-1} is related to the stretching of carbonyl groups, C=O bonds, in the structure of GO. Moreover, the presence of the characteristic peaks at 1050 cm^{-1} , corresponding to C–O bonds, and the broad peak at 3200 cm^{-1} , responsible for OH bonds, is further evidence of GO oxidation.^{3,31,32}

In the spectra of GO-g-PEG400 and GO-g-PEG10000, the characteristic peaks in GO are shifted, which is a sign of

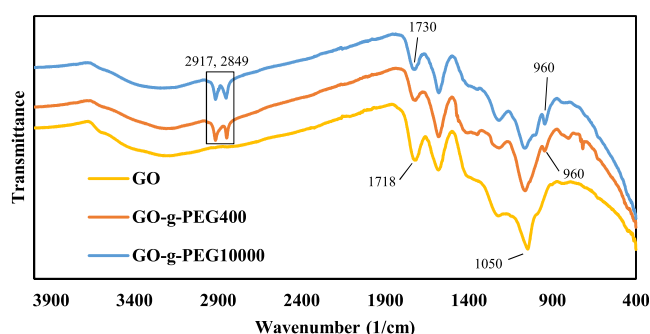


Figure 3. FTIR spectra of GO, GO-g-PEG400, and GO-g-PEG10000.

grafting of PEG chains on the surface of GO.^{3,31} For example, the characteristic peak of C=O bonds at 1718 cm^{-1} was shifted to 1730 cm^{-1} . This shift is a sign of ester group formation due to the reaction between carboxylic groups of GO with hydroxyl end groups of PEG chains.^{15,27} Moreover, the appearance of new peaks at 2917 and 2849 cm^{-1} , arising from the alkyl groups in PEG chains, and the peak at 960 cm^{-1} , due to C–O–C stretching in PEG chains, confirms the reaction between GO and PEG chains.^{3,31}

In the present study, TGA was used to evaluate the graft densities of PEGs of different chain lengths on the surface of GO. Figure 4 displays the TGA of GO, GO-g-PEG400, GO-g-PEG2000, and GO-g-PEG10000 nanoparticles.

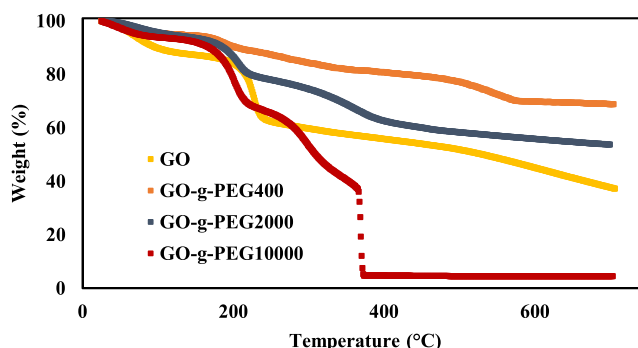


Figure 4. TGA curves of GO, GO-g-PEG400, GO-g-PEG2000, and GO-g-PEG10000.

Using the data presented in Figure 4, one can extract the mass fraction of PEG grafted on the nanoparticles, X_p , which is the weight loss occurring between 250 and 400 °C.³³ From the value of X_p and the total mass of the nanoparticles ($m_p + m_G$) using eq 1, we calculated the mass of PEG, m_p

$$m_p = X_p \times m_{\text{total}} \quad (1)$$

Subsequently, the graphene mass, m_G , is obtained by subtraction of m_p from the total mass:

$$m_G = m_{\text{total}} - m_p \quad (2)$$

From the measured PEG-bonded mass on the nanoparticles and the graphene mass using eqs 1 and 2, the graft density (the number of PEG chains per graphene surface area), N , can be calculated using eq 3³³

$$N = \frac{M}{A} \frac{m_p}{m_G} \frac{1}{M_{W,P}} \quad (3)$$

where $\frac{M}{A}$ is the mass per unit surface area of a GO sheet and $M_{w,p}$ is the molecular weight of PEG in kg/molecule.

The mass per unit surface area of a GO sheet, $\frac{M}{A}$, was calculated based on the mass per surface area of a graphene sheet, which is 7.7×10^{-7} kg/m².³³ In the graphene structure, the length of the C–C bond is 0.142 nm. By considering a hexagonal cell as the repeating structure in graphene, the area of each hexagon is 0.0523 nm², which corresponds to two full atoms of carbon ($1/3 \times 6$). In the case of GO, the mass per unit surface area was calculated by taking the oxidation percentage into account.

As shown in Figure 4, the second mass loss in the thermogram of GO, around 200 °C, indicates the pyrolysis of oxygen-containing groups,^{32,34} which in this case is around 26%. Therefore, the mass per unit surface area of GO was calculated assuming 74% carbon and 26% oxygen in each hexagonal cell using the following formula:

$$\frac{M}{A} = \frac{2 \times ((0.74 \times 1.994 \times 10^{-26}) + (0.26 \times 2.6 \times 10^{-26})) \text{Kg}}{0.0523 \times 10^{-18} \text{m}^2} = 8.225 \times 10^{-7} \text{kg/m}^2 \quad (4)$$

The calculated value of $\frac{M}{A}$ was used in eq 3 to obtain the graft density per unit surface area presented in Table 2.

Table 2. Graft Density of Different PEG Chain Lengths on the Surface of Graphene

sample	X_p (%)	$\frac{m_p}{m_G}$	graft density (chain per nm ²)
PEG400	8	0.07	0.17
PEG2000	17	0.2	0.050
PEG10000	26	0.33	0.016

The table indicates that the graft density decreases sharply with increasing PEG molecular weight. This can be easily understood if we remember that as the molecular weight

increases, the radius of gyration of PEG chains increases, resulting in more steric hindrance for PEG end groups to reach out to the functional groups of GO, resulting, therefore, in a smaller graft density.³⁵

3.2. Dispersion of Nanoparticles. It is well known that in nanocomposites containing graphene, due to a strong π – π interaction between the platelets of GNP, it is difficult to reach an appropriate dispersion of nanoparticles in the polymer matrix. Concomitantly, the dispersion of nanoparticles directly affects the nucleation and final crystallinity of the polymer matrix. Therefore, it is expected that the dispersion of graphene may affect the crystallinity of the PLLA nanocomposites.

To achieve a better insight into both microdispersion and nanodispersion states of PEG-grafted nanoparticles inside PLLA, both optical microscopy (OM) and FE-SEM were used to observe the samples obtained in this work. Figure 5 presents OM and FE-SEM images of PLLA containing 1.5 wt % of GO-g-PEG2000 and GO-g-PEG10000.

A quick comparison between Figure 5a and e seems to indicate that GO-g-PEG10000 is better dispersed with PLLA than GO-g-PEG2000. In the sample containing 1.5 wt % of GO-g-PEG10000, as shown in Figure 5e, nanoparticles disperse in the whole area, while in 2000-1.5, as shown in Figure 5a, nanoparticles form big agglomeration.

From Figure 5b,c,f,g, it can be seen that the number of detected particles in the sample containing GO-g-PEG10000 is larger than for nanocomposites filled with GO-g-PEG2000, indicating a better dispersion of GO in the presence of long chains of PEG10000. Additionally, the size of detected particles is smaller in the sample containing GO-g-PEG10000, which is another evidence of better dispersion of particles in this sample, as shown in Figure 5c,d,g,h.

Moreover, the fracture surface of PLLA containing GO-g-PEG10000 is entirely different from the other nanocomposites. This may be related to more interaction between PLLA and PEG10000 chains in the corresponding sample, inducing a

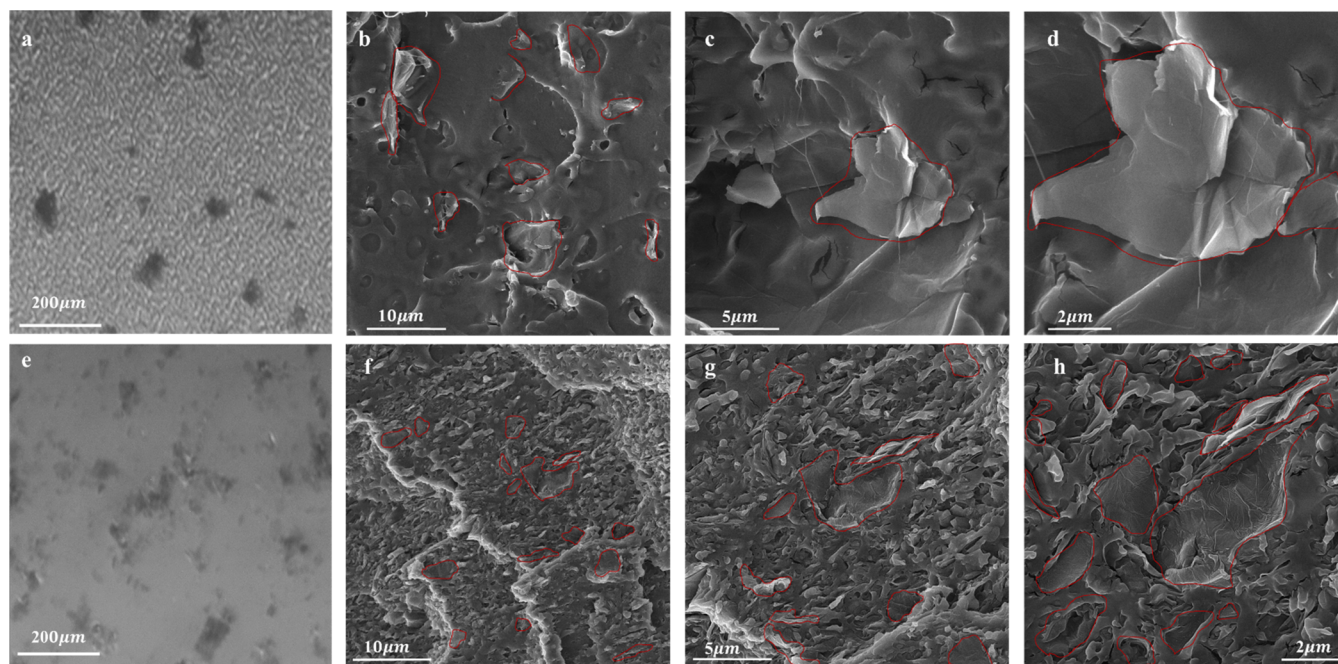


Figure 5. (a) OM image and (b–d) FE-SEM images of the 2000-1.5 sample. (e) OM image and (f–h) FE-SEM images of the 10000-1.5 sample.

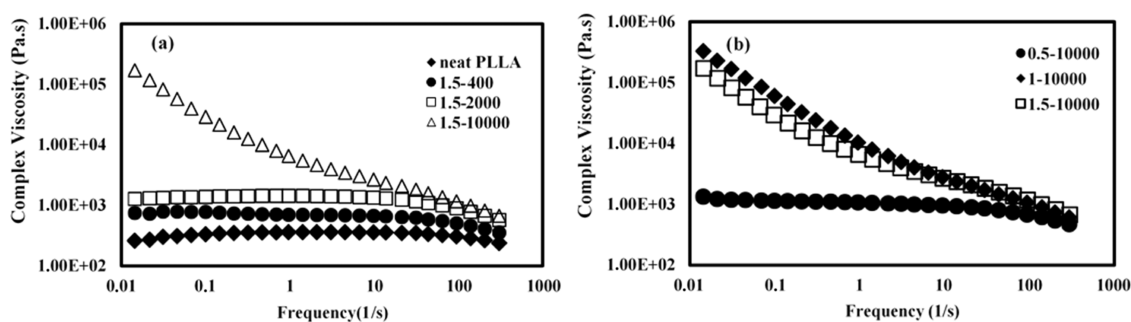


Figure 6. (a) Comparison between the complex viscosity of PLLA nanocomposites containing 1.5 wt % of GO-g-PEG400, GO-g-PEG2000, and GO-g-PEG10000. (b) Complex viscosity of PLLA containing 0.5, 1, and 1.5 wt % of GO-g-PEG10000.

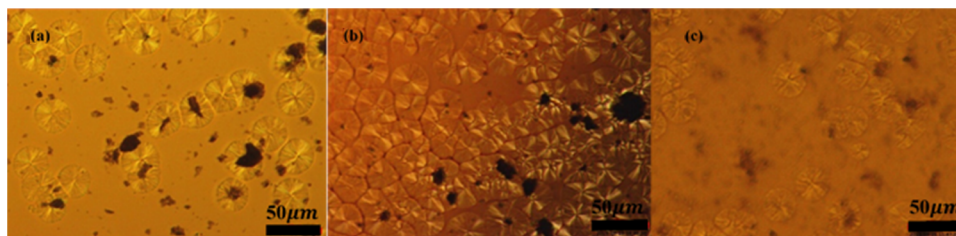


Figure 7. POM images of (a) 400-1, (b) 2000-1, and (c) 10000-1.

ductile fracture behavior in the PLLA matrix. A similar behavior was reported at the interface between the epoxy and GO grafted with different chain lengths of polyetheramine.³⁶

For further investigation on the morphology and dispersion of nanoparticles, rheological measurements were used. Figure 6 presents typical results of the rheological behavior of samples studied in this work. Figure 6a shows the effect of the PEG chain length on the complex viscosity as a function of the frequency for the samples containing 1.5 wt % of GO-g-PEGs, and Figure 6b presents the effect of the concentration on the complex viscosity as a function of the frequency for the samples containing GO-g-PEG10000.

All of the composites presented a typical Newtonian behavior over a wide range of frequency and a slight shear-thinning behavior at high frequencies except when GO-g-PEG10000 in concentrations of 1 and 1.5 wt % was added to PLLA. In this case, a yield stress was observed at low frequencies, indicating that GO-g-PEG10000 nanoparticles start to form a network³⁷ at these concentrations, which are in good agreement with the results of OM images, as shown in Figure 5e.

Moreover, upon the increase of the PEG chain length, complex viscosity increases corresponding to a better dispersion.

Based on the results obtained from rheology and microscopy, it can be concluded that increasing the length of grafted PEG leads to a better dispersion of nanoparticles, which is a result of more interaction between PLLA and PEG chains with increasing PEG chain length. Also, the long chains in PEG10000 could make a bridge between nanoparticles and form a connected structure through the PLLA matrix, as we can see in the form of viscosity upturn in the rheological results and OM image, as shown in Figure 5e.

3.3. Isothermal Crystallization Behavior of PLLA Nanocomposites. Figure 7 presents typical POM images of PLLA nanocomposites during isothermal crystallization at a temperature of 130 °C. In this case, the effect of the PEG chain length on the nucleation density of the PLLA samples

containing 1 wt % GO-g-PEG400, GO-g-PEG2000, and GO-g-PEG10000, after 500s from the beginning of the experiment, is shown.

The POM images clearly illustrate the effect of the PEG chain length on nucleation. By comparing different nanocomposites, it can be seen that PLLA containing GO-g-PEG2000 shows the highest nucleation density.

Table 3 shows the nucleation density and crystal growth rate for all the samples studied in this work at a crystallization temperature (T) of 130 °C.

Table 3. Nucleation Density and Crystal Growth Rate for Samples Studied in This Work at 130 °C

sample	nucleation density ($\times 10^{-2} \mu\text{m}^{-2}$)	crystal growth rate ($\times 10^{+2} \mu\text{m/s}$)
neat PLLA	1.9 ± 0.2	3.8 ± 0.2
400-0.5	3.3 ± 0.5	3.0 ± 0.2
400-1	6.04 ± 0.9	3.1 ± 0.2
400-1.5	8.5 ± 0.4	2.9 ± 0.09
2000-0.5	13.5 ± 1	5.5 ± 0.2
2000-1	17.1 ± 1.2	4.8 ± 0.2
2000-1.5	4.7 ± 0.4	5.1 ± 0.1
10 000-0.5	3.8 ± 0.6	3.5 ± 0.08
10 000-1	6.2 ± 0.8	3.0 ± 0.2
10 000-1.5	4.3 ± 0.6	3.2 ± 0.3

Figure 8a,b shows typical heat flow curves and relative crystallinity as a function of time during isothermal crystallization obtained in this work. In this case, the behavior for the PLLA to which GO-g-PEG400 was added at a temperature of 130 °C, is shown. These curves were used to infer the crystallization induction time, called the onset time, for all the samples studied in this work.

Table 4 presents the crystallization induction time, called the onset time, for all the samples studied in this work at a temperature of 130 °C. This value is taken from the heat flow curves as the time value at which the heat flow starts to

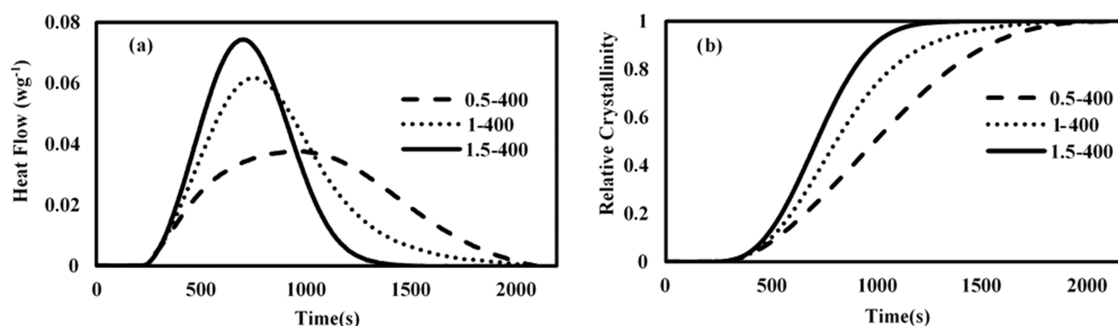


Figure 8. (a) Heat flow curves and (b) relative crystallinity of PLLA containing 0.5, 1, and 1.5 wt % of G-g-PEG400.

Table 4. Thermal Properties of PLLA Nanocomposites at $T = 130\text{ }^{\circ}\text{C}$

sample	t_0 (s)	$t_{0.5}^{-1}$ ($\times 10^3\text{ s}^{-1}$)
neat PLLA	252	0.6
400-0.5	213	1.0
400-1	216	1.2
400-1.5	222	1.4
2000-0.5	147	1.8
2000-1	132	1.5
2000-1.5	135	1.9
10 000-0.5	189	1.2
10 000-1	177	0.8
10 000-1.5	237	0.9

increase, indicating the onset of crystallization at a certain temperature. Table 4 also presents the inverse of the half-time of crystallization, referred to in the present paper as the overall crystallization rate, which is inferred from Figure 8b for all the samples presented in this work. It was observed that for each specific concentration and chain length, the onset time decreased and the crystallization rate increased as expected.

The results presented in Tables 3 and 4 clearly indicate the successful role of GO-g-PEG as a nucleating agent as it increases the nucleation density and crystallization rate. The increase in the concentration of nanoparticles for a constant chain length results in a monotonic increase of the nucleation density for GO-g-PEG400, whereas it results in a maximum at a concentration of 1 wt % for both GO-g-PEG2000 and GO-g-PEG10000. Also, upon the increase of the concentration of nanoparticles, the spherulite growth rate and crystallization rates are constant within an experimental error. The only exception is for GO-g-PEG10000, for which the crystallization rate decreases with the increase of the nanoparticle concentration. Upon the increase of the PEG chain length for a constant nanoparticle concentration, the nucleation density, spherulite growth rate, and crystallization rate manifest a maximum and the induction time a minimum for a PEG chain length of 2000. All of these results can be explained in light of the particle dispersion and PLLA chain mobility as discussed below.

4. DISCUSSION

Upon the increase of the nanoparticle concentration, more sites of nucleation are expected, as is observed experimentally for GO-g-PEG400. However, as the concentration of the nanoparticles increases above 1 wt % for GO-g-PEG2000 and GO-g-PEG10000, the nucleation density decreases most likely due to the steric hindrance between the hairy particles which

are coming closer. This steric hindrance could also explain the reason for the decrease of the crystallization rate observed for GO-g-PEG10000 at concentrations of 1 and 1.5 wt %.

The crystallization process consists of two steps: nucleation and crystal growth. The PEG chain length affects both the steps in the following ways.

The PEG chain length affects the nucleation in two ways: dispersion and steric accessibility to the PLLA chains. In terms of dispersion, our results showed that the longer the PEG chain length (the closer it is to the PLLA chain length), the better the dispersion, and consequently the nucleation. On the other hand, the longer PEG chain, grafted to GO, lessens its effect as a nucleating agent, due to the steric hindrance effect.

Furthermore, the PEG chains impact the local mobility of the adjacent PLLA chains needed to organize in the crystal lamella. A certain mobility range is required for the optimal crystal growth, above and below which the crystal growth is impeded. The effect of the chain length on the crystal growth is analogous to that of temperature.

For GO-g-PEG400, short PEG400 leads to a worse dispersion of the nanoparticles, lessening their role as nucleating agents compared to that of GO-g-PEG2000 for a similar concentration. PEG400 provides more free volume and very high mobility for the PLLA chains. In this case, the PLLA chain mobility is higher than the optimal range preventing the PLLA chains from organizing into a lamellar structure and consequently resulting in a lower crystal growth rate.

Conversely, for GO-g-PEG10000, long PEG10000 chains induce a steric hindrance effect that reduces the accessibility of the nanoparticles to the PLLA chains decreasing the nucleation. This steric hindrance, also, increases the induction time.

The long chains in GO-g-PEG10000 reduce the mobility of the PLLA chains below the optimal range, as demonstrated by the upturn in the viscosity, as shown in Figure 6, leading again to a lower crystal growth rate.

These results strongly confirm that there is an optimal PEG chain length for the best mobility, and hence the crystal growth rate, balancing steric hindrance, and dispersion, resulting in the best nucleation. Therefore, among the investigated chain lengths, PEG2000 yielded the highest crystal growth and nucleation for PLLA.

5. CONCLUSIONS

In this work, the effect of the addition of graphene oxide grafted with different chain lengths of PEG on the crystallinity of PLLA was investigated. The experimental results led us to conclude that it is possible to control the dispersion of GO within PLLA by tailoring the length of the PEG chain that is

grafted on GO: a PEG chain length of 10000 resulted in a better dispersion than a PEG chain length of 400 or 2000. It is also possible to control the PLLA crystal nucleation and growth rate, to which modified GO has been added, by changing the chain length of PEG. Indeed, the PLLA crystal nucleation and growth rate are controlled by the steric hindrance induced by the PEG chain around graphene oxide and PLLA chain mobility. A PEG molecular weight of 2000 g/mol resulted in the highest nucleation density and crystal growth rate in PLLA due to a good balance between the steric hindrance, chain mobility, and dispersion induced in the presence of this chain length.

AUTHOR INFORMATION

Corresponding Authors

Foroud Abbassi-Sourki – Faculty of Processing, Iran Polymer and Petrochemical Institute, Tehran 14965/115, Iran;
Email: f.abbasi@ippi.ac.ir

Nicole.R Demarquette – Department of Mechanical Engineering, École de Technologie Supérieure, Montreal, Québec H3C 1K3, Canada; Email: NicoleR.Demarquette@etsmtl.ca

Authors

Samira Karimi – Faculty of Processing, Iran Polymer and Petrochemical Institute, Tehran 14965/115, Iran;
Department of Mechanical Engineering, École de Technologie Supérieure, Montreal, Québec H3C 1K3, Canada

Ismail Ghasemi – Faculty of Processing, Iran Polymer and Petrochemical Institute, Tehran 14965/115, Iran;
orcid.org/0000-0002-6024-7895

Mazen Samara – Department of Mechanical Engineering, École de Technologie Supérieure, Montreal, Québec H3C 1K3, Canada

Complete contact information is available at:
<https://pubs.acs.org/10.1021/acsomega.2c03397>

Notes

The authors declare no competing financial interest.

ACKNOWLEDGMENTS

The authors would like to acknowledge the financial support of Iran Polymer and Petrochemical Institute (IPPI) and National Science and Engineering Research Council of Canada (NSERC).

REFERENCES

- (1) Yang, J. H.; Shen, Y.; He, W. D.; Zhang, N.; Huang, T.; Zhang, J. H.; Wang, Y. Synergistic effect of poly (ethylene glycol) and graphene oxides on the crystallization behavior of poly (l-lactide). *J. Appl. Polym. Sci.* **2013**, *130*, 3498–3508.
- (2) Sun, Y.; He, C. Synthesis and stereocomplex crystallization of poly (lactide)–graphene oxide nanocomposites. *ACS Macro Lett.* **2012**, *1*, 709–713.
- (3) Zhang, C.; Wang, L.; Zhai, T.; Wang, X.; Dan, Y.; Turng, L.-S. The surface grafting of graphene oxide with poly (ethylene glycol) as a reinforcement for poly (lactic acid) nanocomposite scaffolds for potential tissue engineering applications. *J. Mech. Behav. Biomed. Mater.* **2016**, *53*, 403–413.
- (4) Pei, A.; Zhou, Q.; Berglund, L. A. Functionalized cellulose nanocrystals as biobased nucleation agents in poly (l-lactide)–(PLLA)–Crystallization and mechanical property effects. *Compos. Sci. Technol.* **2010**, *70*, 815–821.
- (5) Wu, D.; Cheng, Y.; Feng, S.; Yao, Z.; Zhang, M. Crystallization behavior of polylactide/graphene composites. *Ind. Eng. Chem. Res.* **2013**, *52*, 6731–6739.
- (6) Ouchiar, S.; Stoclet, G.; Cabaret, C.; Gloaguen, V. Influence of the filler nature on the crystalline structure of polylactide-based nanocomposites: new insights into the nucleating effect. *Macromolecules* **2016**, *49*, 2782–2790.
- (7) Guo, Q. *Polymer Morphology: Principles, Characterization, and Processing*; John Wiley & Sons: New Jersey, 2016; pp 170–200.
- (8) Hu, X.; An, H.; Li, Z.-M.; Geng, Y.; Li, L.; Yang, C. Origin of carbon nanotubes induced poly (L-lactide) crystallization: surface induced conformational order. *Macromolecules* **2009**, *42*, 3215–3218.
- (9) Barrau, S.; Vanmansart, C.; Moreau, M.; Addad, A.; Stoclet, G.; Lefebvre, J.-M.; Seguela, R. Crystallization behavior of carbon nanotube– polylactide nanocomposites. *Macromolecules* **2011**, *44*, 6496–6502.
- (10) Hadaeghnia, M.; Ahmadi, S.; Ghasemi, I.; Wood-Adams, P. M. Manipulating the morphology of PA6/POE blends using graphene to achieve balanced electrical and mechanical properties. *Compos. Sci. Technol.* **2020**, *200*, No. 108412.
- (11) Nofar, M.; Tabatabaei, A.; Park, C. B. Effects of nano-/micro-sized additives on the crystallization behaviors of PLA and PLA/CO₂ mixtures. *Polymer* **2013**, *54*, 2382–2391.
- (12) Day, M.; Nawaby, A.; Liao, X. A DSC study of the crystallization behaviour of polylactic acid and its nanocomposites. *J. Therm. Anal. Calorim.* **2006**, *86*, 623–629.
- (13) Huang, H.-D.; Zhou, S.-Y.; Zhou, D.; Ren, P.-G.; Xu, J.-Z.; Ji, X.; Li, Z.-M. Highly Efficient “Composite Barrier Wall” Consisting of Concentrated Graphene Oxide Nanosheets and Impermeable Crystalline Structure for Poly (lactic acid) Nanocomposite Films. *Ind. Eng. Chem. Res.* **2016**, *55*, 9544–9554.
- (14) Valapa, R. B.; Pugazhenthig, G.; Katiyar, V. Effect of graphene content on the properties of poly (lactic acid) nanocomposites. *RSC Adv.* **2015**, *5*, 28410–28423.
- (15) Zhang, S.; Xiong, P.; Yang, X.; Wang, X. Novel PEG functionalized graphene nanosheets: enhancement of dispersibility and thermal stability. *Nanoscale* **2011**, *3*, 2169–2174.
- (16) Xu, H.; Xie, L.; Wu, D.; Hakkarainen, M. Immobilized graphene oxide nanosheets as thin but strong nanointerfaces in biocomposites. *ACS Sustainable Chem. Eng.* **2016**, *4*, 2211–2222.
- (17) Mekonnen, T.; Mussone, P.; Khalil, H.; Bressler, D. Progress in bio-based plastics and plasticizing modifications. *J. Mater. Chem. A.* **2013**, *1*, 13379–13398.
- (18) Martin, O.; Averous, L. Poly (lactic acid): plasticization and properties of biodegradable multiphase systems. *Polymer* **2001**, *42*, 6209–6219.
- (19) Xiao, H.; Lu, W.; Yeh, J. T. Effect of plasticizer on the crystallization behavior of poly (lactic acid). *J. Appl. Polym. Sci.* **2009**, *113*, 112–121.
- (20) Pillin, I.; Montrelay, N.; Grohens, Y. Thermo-mechanical characterization of plasticized PLA: Is the miscibility the only significant factor? *Polymer* **2006**, *47*, 4676–4682.
- (21) Piorkowska, E.; Kulinski, Z.; Galeski, A.; Masirek, R. Plasticization of semicrystalline poly (L-lactide) with poly (propylene glycol). *Polymer* **2006**, *47*, 7178–7188.
- (22) Xiao, H.; Yang, L.; Ren, X.; Jiang, T.; Yeh, J. T. Kinetics and crystal structure of poly (lactic acid) crystallized nonisothermally: effect of plasticizer and nucleating agent. *Polym. Compos.* **2010**, *31*, 2057–2068.
- (23) Li, H.; Huneault, M. A. Effect of nucleation and plasticization on the crystallization of poly (lactic acid). *Polymer* **2007**, *48*, 6855–6866.
- (24) Liu, C.; Ye, S.; Feng, J. Promoting the dispersion of graphene and crystallization of poly (lactic acid) with a freezing-dried graphene/PEG masterbatch. *Compos. Sci. Technol.* **2017**, *144*, 215–222.
- (25) Xu, H.; Xie, L.; Jiang, X.; Li, X.-J.; Li, Y.; Zhang, Z.-J.; Zhong, G.-J.; Li, Z.-M. Toward stronger transcrystalline layers in poly (L-

lactic acid)/natural fiber biocomposites with the aid of an accelerator of chain mobility. *J. Phys. Chem. B* **2014**, *118*, 812–823.

(26) Xu, J.-Z.; Zhang, Z.-J.; Xu, H.; Chen, J.-B.; Ran, R.; Li, Z.-M. Highly enhanced crystallization kinetics of poly (l-lactic acid) by poly (ethylene glycol) grafted graphene oxide simultaneously as heterogeneous nucleation agent and chain mobility promoter. *Macromolecules* **2015**, *48*, 4891–4900.

(27) Karimi, S.; Ghasemi, I.; Abbassi-Sourki, F. A study on the crystallization kinetics of PLLA in the presence of Graphene Oxide and PEG-grafted-Graphene Oxide: Effects on the nucleation and chain mobility. *Composites, Part B* **2019**, *158*, 302–310.

(28) Dikin, D. A.; Stankovich, S.; Zimney, E. J.; Piner, R. D.; Dommett, G. H.; Evmenenko, G.; Nguyen, S. T.; Ruoff, R. S. Preparation and characterization of graphene oxide paper. *Nature* **2007**, *448*, 457–460.

(29) Chen, J.; Li, Y.; Huang, L.; Li, C.; Shi, G. High-yield preparation of graphene oxide from small graphite flakes via an improved Hummers method with a simple purification process. *Carbon* **2015**, *81*, 826–834.

(30) Guerrero-Contreras, J.; Caballero-Briones, F. Graphene oxide powders with different oxidation degree, prepared by synthesis variations of the Hummers method. *Mater. Chem. Phys.* **2015**, *153*, 209–220.

(31) Jayan, J. S.; Saritha, A.; Deeraaj, B. D. S.; Joseph, K. Graphene oxide as a prospective graft in polyethylene glycol for enhancing the toughness of epoxy nanocomposites. *Polym. Eng. Sci.* **2020**, *60*, 773–781.

(32) Gomari, S.; Ghasemi, I.; Esfandeh, M. Effect of polyethylene glycol-grafted graphene on the non-isothermal crystallization kinetics of poly (ethylene oxide) and poly (ethylene oxide): lithium perchlorate electrolyte systems. *Mater. Res. Bull.* **2016**, *83*, 24–34.

(33) Chadwick, R. C.; Khan, U.; Coleman, J. N.; Adronov, A. Polymer Grafting to Single-Walled Carbon Nanotubes: Effect of Chain Length on Solubility, Graft Density and Mechanical Properties of Macroscopic Structures. *Small* **2013**, *9*, 552–560.

(34) Niyogi, S.; Bekyarova, E.; Itkis, M. E.; McWilliams, J. L.; Hamon, M. A.; Haddon, R. C. Solution properties of graphite and graphene. *J. Am. Chem. Soc.* **2006**, *128*, 7720–7721.

(35) Lai, X. L.; Yang, W.; Wang, Z.; Shi, D. W.; Liu, Z. Y.; Yang, M. B. Enhancing crystallization rate and melt strength of PLLA with four-arm PLLA grafted silica: The effect of molecular weight of the grafting PLLA chains. *J. Appl. Polym. Sci.* **2018**, *135*, 45675.

(36) Guan, L.-Z.; Wan, Y.-J.; Gong, L.-X.; Yan, D.; Tang, L.-C.; Wu, L.-B.; Jiang, J.-X.; Lai, G.-Q. Toward effective and tunable interphases in graphene oxide/epoxy composites by grafting different chain lengths of polyetheramine onto graphene oxide. *J. Mater. Chem. A* **2014**, *2*, 15058–15069.

(37) Hadaeghnia, M.; Ahmadi, S.; Ghasemi, I.; Wood-Adams, P. M. Evolution of Phase Morphology, Rheology, and Electrical Conductivity of PA6/POE Blends Containing Graphene during Annealing under SAOS. *Macromolecules* **2022**, *55*, 2714–2728.

Recommended by ACS

Toward Heat-Resistant and Transparent Poly(l-lactide) by Tailoring Crystallization with an Aliphatic Amide as a Nucleating Agent

Xiaonan Chen, Hongwei Bai, *et al.*

SEPTEMBER 06, 2022

INDUSTRIAL & ENGINEERING CHEMISTRY RESEARCH

READ 

Structure Evolution of Oriented Poly(l-lactic acid) Ultrathin Films during Deformation

Yunpeng Li, Shouke Yan, *et al.*

JULY 28, 2022

MACROMOLECULES

READ 

Fabrication of UV- and Heat-Resistant PDLA/PLLA-g-Nanolignin Composite Films by Constructing Interfacial Stereocomplex Crystallites

Weijun Yang, Piming Ma, *et al.*

NOVEMBER 15, 2021

ACS SUSTAINABLE CHEMISTRY & ENGINEERING

READ 

Fully Bio-Based and Supertough PLA Blends via a Novel Interlocking Strategy Combining Strong Dipolar Interactions and Stereocomplexation

Xiangjian Chen, Yueheng Li, *et al.*

JUNE 24, 2022

MACROMOLECULES

READ 

Get More Suggestions >